Investigating the Sintering Process and Mechanical Properties of Nano-copper Particles Coupling Particle Packing Modeling with Molecular Dynamics Simulation

Liu, Xu ; Hu, Dong; Li, Zichuan; Fan, Xuejun; Zhang, Guoqi ; Fan, Jiajie

Citation (APA)
Liu, X., Hu, D., Li, Z., Fan, X., Zhang, G., & Fan, J. (2024). Investigating the Sintering Process and Mechanical Properties of Nano-copper Particles Coupling Particle Packing Modeling with Molecular Dynamics Simulation. In *Proceedings of the 2024 25th International Conference on Thermal, Mechanical and Multi-Physics Simulation and Experiments in Microelectronics and Microsystems (EuroSimE)* (2024 25th International Conference on Thermal, Mechanical and Multi-Physics Simulation and Experiments in Microelectronics and Microsystems, EuroSimE 2024). IEEE. https://doi.org/10.1109/EuroSimE60745.2024.10491446

Important note
To cite this publication, please use the final published version (if applicable).
Please check the document version above.

Investigating the Sintering Process and Mechanical Properties of Nano-copper Particles Coupling Particle Packing Modeling with Molecular Dynamics Simulation

Xu Liu[1], Dong Hu[2], Zichuan Li[2], Xuejun Fan[4], Guoqi Zhang[2], Jiajie Fan [1,2,3*]

1 Academy for Engineering & Technology; Shanghai Engineering Technology Research Center for SiC Power Device, Fudan University, Shanghai 200433, China

2 EEMCS Faculty, Delft University of Technology, Delft, the Netherlands

3 Research Institute of Fudan University in Ningbo, Ningbo 316336, China

4 Department of Mechanical Engineering, Lamar University, Beaumont, TX 77710, USA

*Corresponding: Jiajie Fan (Fudan University), Email: jiajie_fan@fudan.edu.cn

Abstract

The nano-copper particles are widely used in the sintering processes of packaging wide bandgap semiconductors. Despite the significant success in the industry, the mechanism bridging the sintering process to the mechanical properties of sintered nano-copper is not yet well-modeled. In this paper, the impacts of different sintering temperatures and initial porosities caused by different stacking patterns on the uniaxial tensile performance of the sintered layer were studied via a molecular dynamics approach. Two stacking patterns, simple cubic and face-centered cubic, were simulated, respectively. Evolution of their structure at temperatures of 300, 400, 500, and 600 K were simulated as the sintering process. Afterward, the sintered structures were subjected to uniaxial tensile with rates of 0.01 and 0.04 Å/ps at different temperatures to compare the mechanical properties. The results show that the sintering rate and density of the sintered structure increase with a higher temperature. However, the tensile strength of the sintered structure is less relevant to the difference in stacking pattern. This study proves that porosity has a greater effect on sintering quality.

Keywords: Nano-copper sintering; molecular dynamics simulation; particle packing model; tensile simulation

1. Introduction

Wide-bandgap semiconductor (WBS) power devices are leading to higher power density, lower losses, higher frequencies, and higher temperature applications [1]. This brings new challenges to the reliability of module packaging. Because of their larger surface-to-volume ratio and surface curvature, nano-scale metal particle sintering materials offer better electrical interconnection, mechanical support, and heat dissipation channels upon packaging [2]. Thus, they can achieve low-temperature packaging, and high-temperature service for WBSs [3].

Nano-silver sintering materials have been widely studied as a new generation of packaging and interconnection materials. They have unique thermal, electrical, and mechanical properties, but their high price also inevitably limits application [4-6]. In the meantime, with higher melting temperature, anti-electromigration ability, and higher thermal conductivity, nano-copper sintering materials are expected to become the next-generation bonding and interconnection material for WBS packaging [7,8].

Molecular dynamics (MD) simulation can be used to simulate the molecular motion process during sintering to understand the sintering mechanisms and the mechanical properties of final products [9]. The sintering mechanism of different nanoparticles has been widely studied. For instance, Nandy *et al.* [10] studied the microstructure of aluminium alloy nanoparticles ($AlSi_{10}Mg$) in the laser sintering process using four different spherical, cylindrical, cubic, and diamond prism types. Alarifi *et al.* [11] performed molecular dynamics simulations based on the embedded atom method (EAM) to study the pressure-less sintering kinetics of two Ag NPs. Hu *et al.* [12] performed an MD simulation on the coalescence kinetics and mechanical behavior of pressure-assisted Cu nanoparticles (NPs) sintering at low temperatures. Mingfei Gu *et al.* [13] analyzed the structural evolution of equally sized nanoparticles (EPs) and unequally sized nanoparticles (UPs) during the sintering process alongside morphology changes. Li *et al.* [14] studied the sintering behaviors between Ag NPs and nanoflakes (NF) of the same size via molecular dynamics. Cheng *et al.* [15] studied the sintering of a multi-Cu NPs system at multiple temperatures and pressures. Simulation efforts have been made to connect the sintered structure with mechanical properties. Chen *et al.* [16] investigated the structural evolution of three-dimensional network graphene/copper (3DN-Gr/Cu) composites as well as their influence on mechanical properties.

The NP bonding quality and the mechanical properties of sintered products are closely related. Thus, the sintering quality is often evaluated by the mechanical properties of the sintered bodies [17]. Tavakol *et al.* [18] investigated the mechanical properties of nano-composites produced by shock wave sintering of Al and SiC nano-powders. Zhu *et al.* [19] studied the effect of graphene on the mechanical properties through the tensile process on the sintered composite. Abedini *et al.* [20] evaluated the micro-structural changes within the NPs during the sintering process and tested the temperature-dependent mechanical properties of the final products by employing uniaxial tensile testing. Abedini *et al.* [21] determined the sintering parameters influencing the atomic structure, sintering mechanisms, and elastoplastic properties of sintered Al-Cu nanoparticle composite.

Generally, most prior researches focus on using the double-sphere model to simulate the sintering process of NPs. Here, molecular dynamic simulations were used in this study to compare the sintering mechanism of a multi-sphere model of nano-copper particles with different stacking structures, i.e. simple cube and face-centered cube. MD simulations on these two structures can simply represent the nano-Cu nanoparticle sintering process by considering porosity and temperature effects. The sintering structure with the most compact structure is selected to stretch at different temperatures and different strain rates. Through these simulations, mechanical properties are studied, and the sintering quality is judged. This study provides theoretical support for the nano-copper sintering material and process designs.

2. Methods and modeling

2.1 Atomistic level particle packing modeling

We established nano-copper stacking particles with simple cubic and face-centered cubic alignments in Material Studio. After structural optimization, the atomic position files were exported. The classical EAM used in this study describes the interaction between Cu atoms and can accurately describe Cu atomic properties [21, 22]. The total energy of the system based on this force field is:

$$E_i = F_\alpha \left(\sum_{j \neq i} \rho_\beta \left(r_{ij} \right) \right) + \frac{1}{2} \sum_{j \neq i} \varphi_{\alpha\beta} \left(r_{ij} \right) \qquad (1)$$

Where subscripts α, β indicate the element types; i and j are the indices of atoms. F is the is the embedding function of the sum of electron density ρ, and φ is the pairwise interaction that is a function of the atom types α and β as well as the atomic spacing r_{ij}.

Table 1 shows models of the two different packing structures used in this study. Initially, we set a cubic simulation box with dimensions of 72.294 Å. The simple cubic and face-centered cubic structures were constructed in the simulation box. In the simple cubic structure, we filled it with small spheres of radius 18.0736 Å, with a total of 16744 atoms in the whole structure. The simple cubic structure used in this study is equivalent to a nano-copper structure with a porosity of 48%. In this structure, one small sphere is directly connected to the six small spheres. For the face-centered cubic structure, we filled the box with 21856 atoms in the aligned spheres with a radius of 12.7798 Å. The face-centered cube structure has an initial porosity of 26%. In this structure, one small sphere is directly connected to the twelve small spheres. In order to better present the boundaries between NPs, atoms belong different NPs are colored in different colors to better present the NP-NP boundaries. The simulation results were visualized in the Open Visualization Tool (OVITO).

2.2 Simulation flow

The atomic position files were first imported into the Large-scale Atomic/Molecular Massively Parallel Simulator (LAMMPS). EAM potential was used. Periodic condition was applied to all boundaries. The time step was set as 1 fs. The entire simulation procedure is shown in Figure 1. The sintering period was set to 100 ps so the atoms could reach an equilibrium. After sintering, the entire system is relaxed at stretching temperatures. A tension with a constant strain rate was further applied to the sintering model at different temperatures to evaluate each sintering structure's sintering quality.
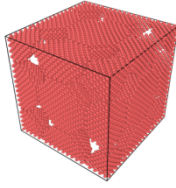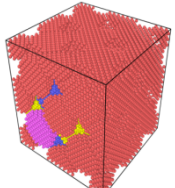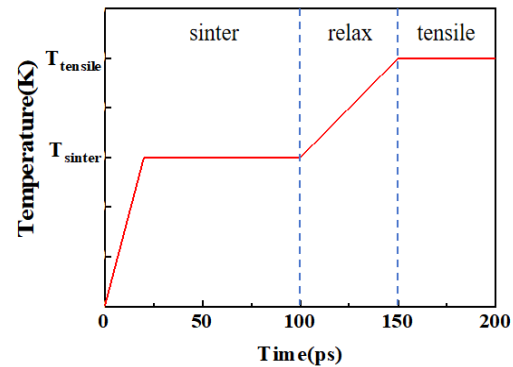

Figure 1. Shear simulation process for nano-Cu sintered model.

Table 1. The details of atomistic models

	Simple Cube	Face-centered Cube
Models		
Atom numbers	16744	21856
Model size	72.294 Å*72.294 Å*72.294 Å	
The radius of the sphere	18.0736 Å	12.7798 Å

2.2.1 Sintering simulation

Considering the high surface energy of the nanoparticles, the whole sintering temperature is relatively low. Thus, 300 K, 400 K, 500 K, and 600 K were selected as the sintering simulation temperature in this study. The sintering process was analyzed via the geometric evolution of different models and the crystal-type transition. The structural evolution can be observed directly. At the microscopic level, dislocation analysis (DXA) and common neighbor analysis (CNA) can identify sintering crystal structures and the defects formed inside [23]. The nano-copper spheres comprising these two structures are different in size. Thus, the number of sintering necks formed is also different. Therefore, this study only qualitatively compared the sintering process of simple cubic and face-centered cubic stacking structures. Mean Squared Displacement (MSD) was calculated to evaluate the entire model's sintering performance and determine the diffusion rate. The formula is as follows:

$$\text{MSD} = \frac{1}{N} \sum_{i=1}^{N} \left[\boldsymbol{r}_i(t) - \boldsymbol{r}_i(0) \right]^2 \qquad (2)$$

Here, N is the number of atoms, and $\boldsymbol{r}_i(t)$ and $\boldsymbol{r}_i(0)$ are the positions of ith atom at time t and time 0, respectively.

2.2.2 Tensile simulation

Figure 2 illustrates the sintered porous structure and the loads. We selected 300 K, 400 K, 500 K, and 600 K as the tensile temperatures, and 0.01 Å/ps and 0.04 Å/ps as the tensile rates. The stress-strain curves of these loading factors were obtained. The failure mechanism of different conditions is studied by analyzing the evolution of different structures and comparing the stress-strain curves.
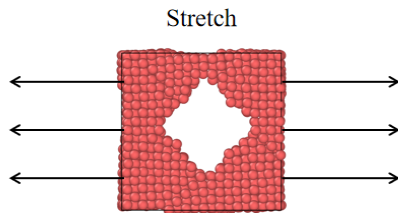

Figure 2. Simple cube model for the tensile simulation.

3. Simulation Results and Discussion

3.1 Sintering simulation

3.1.1 Effect of temperature on the sintering

Here, the sintering results of the models with different stacking structures are analyzed at different temperatures. Figure 3 shows the atomic distribution plots of different models sintered at different temperatures. The number of atoms at different positions is counted at the initial state and after the sintering process. Contrasting the two curves yields the motion trend of the copper atoms. Figure 4 shows a cloud map of the atomic trajectories of different models sintered at different temperatures. The moving distance of each atom was counted and colored according to the distance. The motions of copper atoms at different positions can be analyzed. Figure 5 shows the MSD of different models sintered at different temperatures. For models of simple cubic structure, the mean atomic velocity

and the overall atomic displacement increase with increasing sintering temperature. The significant movement of atoms at the contact point and near the sintering neck contributes to the increased number of atoms in the neck region. Figure 5(a) shows the MSD of the simple cube structure at equilibrium increases with the increasing sintering temperature initially but then decreases at the temperature above 500 K. The optimal temperature for sintering is at 500 K. For the face-centered cubic packing structure model, the overall atomic displacement is the largest. It can eventually form a uniform sintered structure. The MSD of the overall atoms increases with increasing temperature. At the temperature of 600 K, the MSD of the entire sintering structure reaches a maximum.
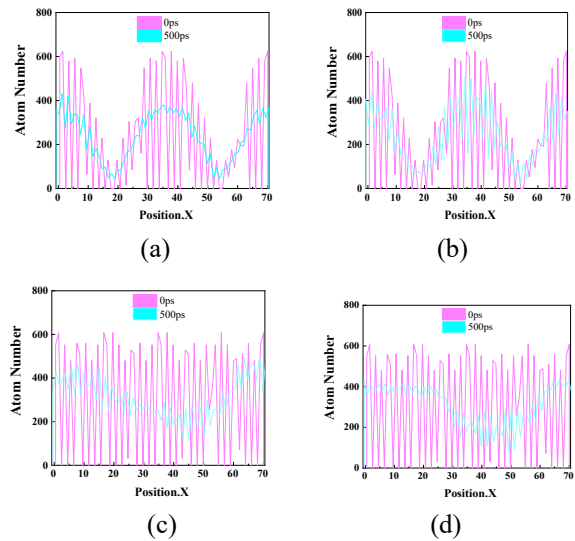

(a)

(b)

(c)

(d)

Figure 3. Atomic distribution map for different models at different sintering temperatures: (a) simple cubic at 300 K; (b) simple cubic at 600 K; (c) face-centered cubic at 300 K; (d) face-centered cubic at 600 K.
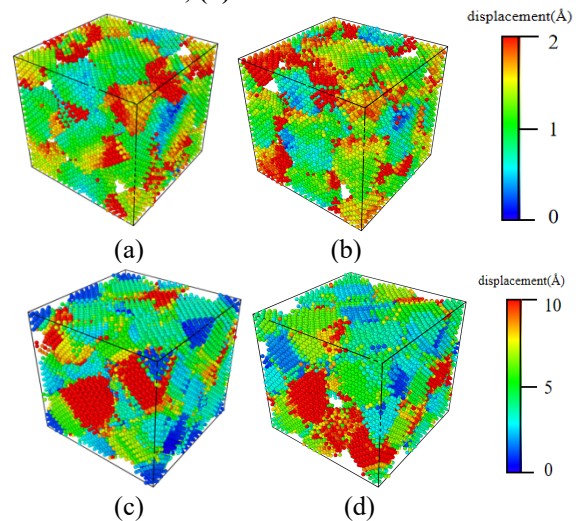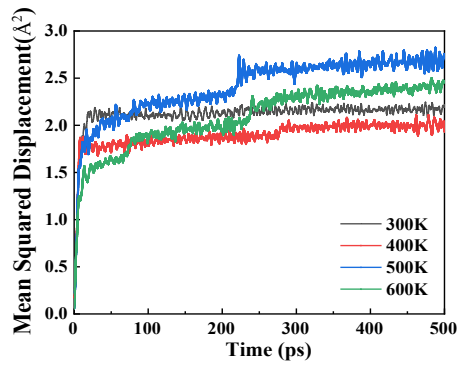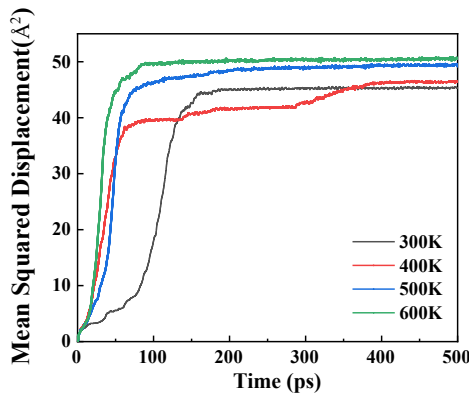

(a)

(b)

(c)

(d)

Figure 4. Cloud map of the atomic motion trajectory for different models at different sintering temperatures: (a) simple cubic at 300 K; (b) simple

cubic at 600 K; (c) face-centered cubic at 300 K; (d) face-centered cubic at 600 K.

(a)

(b)

Figure 5. MSD for different models at different sintering temperatures: (a) simple cubic; (b) face-centered cubic.

3.1.2 Effect of stacking structure on the sintering

Figure 6 shows the results of copper NPs running 500 ps at 600 K. Figure 6(a) shows the evolution of atomic motion and the transformation of the internal crystal structure at different times. For copper nanoparticles with a simple cubic structure, the molecules move stepwise during the sintering process and finally form a stable configuration. The simple cubic structure has three complete contact points in the initial state, and the atoms move and diffuse at these three contact points during the sintering process. By analyzing the atomic crystal structure changes during sintering, we find that the copper atoms diffuse away from the initial position, changing from FCC to HCP lattice, indicating the existence of dislocations. When running up to 10 ps, we can see that many atomic defects gather at the atomic contact points of the simple cubic structure, forming the surface defects. The place where these defects gather is the sintering neck. The emerging surface defects also accelerate atomic diffusion. When running to 20 ps, the sintered neck is significantly more extensive and closely connected. In the late sintering stage, the diffusion rate of internal atoms significantly decreases, the whole structure reaches a new equilibrium, and the internal defects are significantly reduced until a stable sintering structure is

formed. Figure 6 (b) shows copper NPs' atomic trajectory cloud image in the sintering process. The atomic movement near the sintering neck is the most intense. The atomic movement is subdued in the region away from the sintering neck. Figure 6(c) shows the distribution of atoms in different positions along the x-axis before and after sintering. The distribution of atoms becomes more chaotic with further sintering. This result indicates that the atoms gradually spread along the sintering neck region, making the entire structure denser.
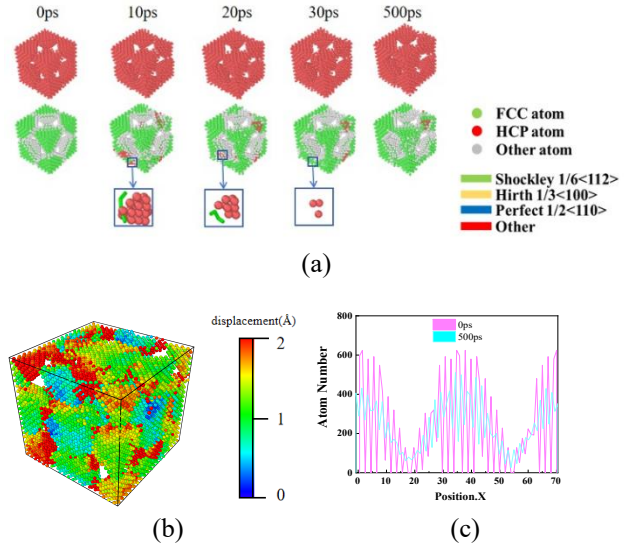

(a)

(b)   (c)

Figure 6. (a) Evolution of snapshots and lattice structure during sintering; (b) cloud map of the atomic motion trajectory; (c) atomic distribution map of a simple cubic structure sintering at 600 K.

Figure 7 presents the results of copper nanoparticles with a face-centered cubic stacking at 500 ps at 600 K. Figure 7(a) shows the process of atomic motion and the transformation of the internal crystal structure at different times. During the starting stage of the sintering process, the atomic diffusion mainly takes place in the sintering neck region, where it was initially the contact point. At 10 ps, significant surface defects at the contact point and more intense atomic diffusion in the sintering neck region. At 40 ps, the sintering neck region was gradually enlarged, the sintered neck formed in two completely contactless NPs in the initial state, and surface defects formed at the sintering neck. As the sintering process proceeds, the whole sintering structure forms a unified whole. When running to 50 ps, we can see the disordered diffusion between the atoms and the formation of multiple point and line defects. When running to 100 ps, the sintering structure forms a more unified sintering structure. Figure 7 (b) shows a cloud diagram of the atomic trajectories of the copper nanoparticles during the sintering process. The atoms throughout the cell are significantly displaced, prompting the whole structure to form a more unified sintering structure. Figure 7(c) shows the distribution of atoms in different positions before and after sintering. Atoms in the face-centered cubic packing model are uniformly arranged

in the simulating box after sintering and become an almost completely dense whole.
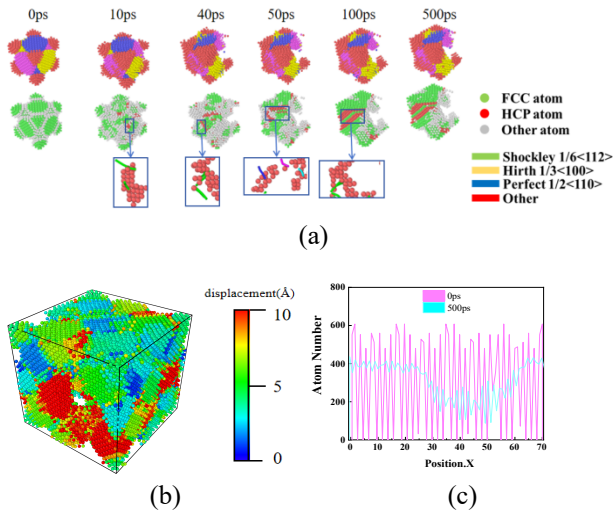

(a)

(b)   (c)

Figure 7. Evolution of (a) snapshots during sintering: lattice structures; (b) cloud map of the atomic motion trajectory; (c) atomic distribution map of a face-centered cubic structure sintering at 600 K.

The simple cubic structure ends up with higher porosity. Atomic diffusion primarily occurs near the sintering neck during the sintering process. The small spheres in the entire simulation box are connected into a whole by a sintered neck. For this structure, the sintering structure is more compact with increasing temperature. For the face-centered cubic stacking structure, the porosity of the whole structure is lower. During the sintering process, the atoms move more violently. During the initial stage of sintering, the atoms near the contact point diffuse with each other, and the sintering neck gradually increases. By the late sintering period, the sintering neck extends between the two spheres that are not in contact at the initial stage, and the atoms in the whole simulation box diffuse with each other to form a more uniformly compact whole. With increasing temperature, the induced density of the sintering structure also increases.

3.2 Tensile simulation

3.2.1 Microstructure analysis of tensile simulations

The analysis above suggested 600 K be the sintering temperature to perform the tensile tests on the sintered structures with different initial stacking structures. The results are used to evaluate the sintering quality of different stacking structures. Figures 8 and 9 show the stretching process of sintered bodies with simple cubic and face-centered cubic stacking structures, respectively. For the simple cubic stacking structure, the density of the sintered structure is low--only the sintering neck of the whole structure is connected. The connection force between the overall sintering structure is relatively small. The sintered structure prefers to break at the sintering neck region during stretching. This sintering structure is connected only by the atoms near the sintering neck, and the inter-atomic bonding is weak so that the NPs are sintered without large deformation. The surface-centered cubic packing structure

model has a sintering structure that is uniformly compact. During stretching, the sintering structure is tightly joined and gradually deformed. There will still be pores in the final sintering structure. The pores gradually expand during the stretching process, and cracks form in the sintering structure, eventually leading to the fracture of the sintered structure.
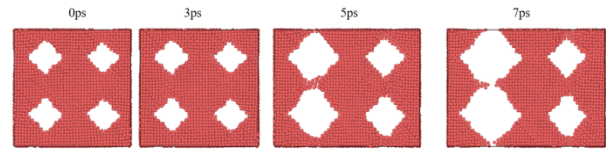

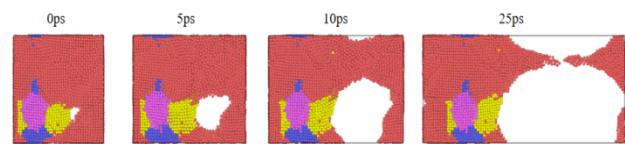***Figure 8. Evolution of simple cubic structure during stretching.***

Figure 9. Evolution of face-centered cubic structure during stretching.

3.2.2 Effects of process parameters on the mechanical properties

We emphasize comparing the stretching results of sintered bodies with different packing structures at different temperatures and strain rates. Figure 10 shows the stress-strain curves of sintered structures with different stacking structures at different temperatures and strain rates. The sintered structure is gradually stretched to break as the force increases.
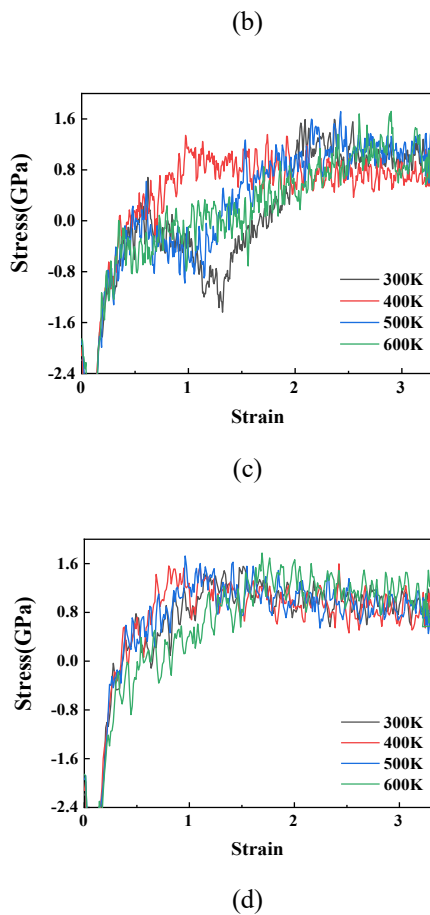

(a)

(b)

(c)

(d)
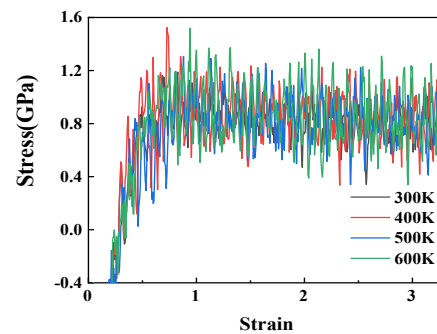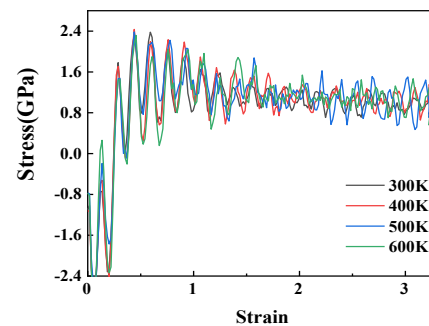
Figure 10. Stress-strain curves at different temperatures. sorted by: (a) simple cubic at 0.01 Å/fs; (b) simple cubic at 0.04 Å/fs; (c) face-centered cubic at 0.01 Å/fs; (d) face-centered cubic at 0.04 Å/fs.

From Figure 10(a), in the case of a low strain rate, the sintered body formed by the simple cubic packing structure has a lower density and tensile strength. From the stress-strain curves, the tensile strength of the sintering structure at the low strain rate is not very responsive to the temperature. From Figure 10(b), in the case of a high strain rate, the simple cubic packing structure has a higher tensile strength. Its tensile strength increases slowly (1.4 to 2.2 GPa) with increasing strain rate. The sintered structure with a simple cubic packing structure has a tensile strength that does not change remarkably at different temperatures. From Figure 10(c), in the case of the face-centered cubic structure, the temperature affects the strain curve at the low strain rate. Its modulus increases first and then decreases with increasing temperature. It reaches the maximum at 400 K. From Figure 10(d), the effect of temperature on the tensile strength is negligible at high strain rates.

4. Conclusions

This study used an EAM-based MD simulation to study the sintering behavior of copper NPs with different stacking structures in the multi-sphere model. The simple cubic stacking structure and a face-centered cubic packing structure were established, and their sintering behaviors were simulated at different temperatures. The rule of atomic movement and the sintering quality of different structures were evaluated by atomic distribution, atomic trajectory cloud map, and MSD. The mechanical performance of different sintered structures was further evaluated by a tensile simulation at different temperatures and strain rates. The simulation showed the following results: firstly, as the porosity of the sintering structure from a simple cubic packing structure is more significant, the sintering structure is only formed by the sintering neck into a whole. Meanwhile, the face-centered cubic structure was formed with a more complete and uniform sintering structure after sintering. For both structures, the sintering quality increased with increasing temperature. Furthermore, in the stretching process on the different sintered structures, the dependence of the tensile strength of sintered bodies on different stacking structures was insignificant. With increasing strain rate and temperature, the tensile strengths of sintered bodies with different packing structures remained essentially unchanged. The sintered neck region broke without large deformation in the simple cubic packing structure model. The internal pores gradually expand during the stretching process and eventually form cracks, leading to a fracture in the sintered body. Generally, this work suggests the different initial stacking patterns of NPs can lead to different failure mechanisms of porous sintered structures.

References
1. Y. Qin et al., "Thermal management and packaging of wide and ultra–wide bandgap power devices: A review and perspective,", Phys. D: Appl.Phys., vol. 66, no. 9, pp. 1–23, 2023.
2. Jiang H, Moon K, Dong H et al. "Size-dependent melting properties of tin nanoparticles. " Chem Phys Lett 2006;429:492e6.
3. Yan H, Liang P, Mei Y, et al. "Brief review of silver sinter-bonding processing for packaging high-temperature power devices. " Chinese Journal of Electrical Engineering, 2020, 6(3): 26-34.
4. Ren L, Li Q, Lu J et al. "Enhanced thermal conductivity for Ag-deposited alumina sphere/epoxy resin composites through manipulating interfacial thermal resistance. " Compos. Part A 2018, 107, 661.
6. Shen W, Zhang X, Huang Q et al. "Preparation of solid silver nanoparticles for inkjet printed flexible electronics with high conductivity. " Nanoscale 2014, 6, 1622.
6. Roy S, Shankar S, Rhim J. "Melanin-mediated synthesis of silver nanoparticle and its use for the preparation of

carrageenan-based antibacterial films. " Food Hydrocoll. 2019, 88, 237.

7. Hsiao C, Kung T, Song J et al. "Development of Cu–Ag pastes for high temperature sustainable bonding," Mater. Sci. Eng., A, vol. 684, pp. Jan. 2017, doi: 10.1016/j.msea.2016.12.084.

8. Y Mou, H Cheng, Y Peng et al. "Fabrication of reliable Cu–Cu joints by low temperature bonding isopropanol stabilized Cu nanoparticles in air," Mater. Lett., vol. 229, pp. Oct. 2018, doi: 10.1016/j.matlet.2018.07.061.

9. Ding L, Davidchack, Pan J. "A Molecular Dynamics Study of Sintering between Nanoparticles. " Comput. Mater. Sci. 2009, 46, 247.

10. Nandy J, Sahoo S, Sarangi H. "Study on shape dependency of Al-alloy nanoparticles during coalescence in direct metal laser sintering: A molecular dynamics approach. " Materials Today-Proceedings, 2021, 41: 347-361.

11. Alarifi H A, Atis M, Ouml, et al. "Molecular Dynamics Simulation of Sintering and Surface Premelting of Silver Nanoparticles. " Materials Transactions, 2013, 64(6): 884-889.

12. D. Hu, Z. Cui, J. Fan, X. Fan, and G. Zhang, "Thermal kinetic and mechanical behaviors of pressure-assisted Cu nanoparticles sintering: A molecular dynamics study," Results in Physics, vol. 19, p. 103486, 2020.

13. Gu M, Liu T, Xiao X et al. "Simulation and Experimental Study of the Multisized Silver Nanoparticles Sintering Process Based on Molecular Dynamics. " Nanomaterials 2022, 12, 1030.

14. S. Li et al., "Sintering mechanism of Ag nanoparticle-nanoflake: a molecular dynamics simulation," journal of materials research and technology, vol. 16, pp. 640-666, 2022

16. B. Cheng and A. H. Ngan, "The sintering and densification behaviour of many copper nanoparticles: A molecular dynamics study," Computational materials science, vol. 74, pp. 1-11, 2013.

16. Chen, CJ et al. "The atomic structure evolution and strengthening mechanism in three-dimensional network graphene enhanced Cu: A molecular dynamics simulation. " Journal of Alloys and Compounds, 963 (2023) 171293

17. S. Yang, W. Kim, M. Cho. "Molecular dynamics study on the coalescence kinetics and mechanical behavior of nanoporous structure formed by thermal sintering of cu nanoparticles, " Int. J. Eng. Sci. 123 (2018) 1–19.

18. M. Tavakol, M. Mahnama, R. Naghdabadi. "Shock wave sintering of Al/SiC metal matrix nano-composites: a molecular dynamics study" Comput. Mater. Sci 126 (2016) 266–262.

19. Zhu Y, Li N, Li W et al. " Atomistic Study on the Sintering Process and the Strengthening Mechanism of Al-Graphene System. " Materials 2022, 16, 2644.

20. A. Abedini, A. Montazeri, A. Malti, A. Kardani. "Mechanical properties are affected by coalescence mechanisms during sintering of metal powders: Case study of Al-Cu nanoparticles by molecular dynamics simulation, " Powder Technology 406 (2022) 117667.

21. A. Abedini, A. Malti, A. Kardani, A. Montazeri. "Probing neck growth mechanisms and tensile properties of sintered multi-nanoparticle Al-Cu systems via MD simulation, " Advanced Powder Technology 34 (2023) 104084.

22. L. Wang et al., "New twinning route in face-centered cubic nanocrystalline metals," Nature communications, vol. 8, no. 1, p. 2142, 2017.

23. A. Stukowski, "Visualization and analysis of atomistic simulation data with OVITO–the Open Visualization Tool," Modelling and simulation in materials science and engineering, vol. 18, no. 1, p .016012, 2009.